CrossMark

$1/f^{\alpha}$ Low Frequency Fluctuations in Turbulent Flows
Transitions with Heavy-Tailed Distributed Interevent Durations

J. Herault[1,2] · **F. Pétrélis**[1] · **S. Fauve**[1]

Abstract We report the experimental observation of low frequency fluctuations with a spectrum varying as $1/f^{\alpha}$ in three different turbulent flow configurations: the large scale velocity driven by a two-dimensional turbulent flow, the magnetic field generated by a turbulent swirling flow of liquid sodium and the pressure fluctuations due to vorticity filaments in a swirling flow. For these three systems, $1/f^{\alpha}$ noise is shown to result from the dynamics of coherent structures that display transitions between a small number of states. The interevent duration is distributed as a power law. The exponent of this power law and the nature of the dynamics (transition between symmetric states or asymmetric ones) select the exponent α of the $1/f^{\alpha}$ fluctuations.

Keywords $1/f$ noise · Turbulence · Rare events

1 Introduction: $1/f$ Noise and Turbulence

Originally observed in different types of electrical conductors [1], $1/f$ noise (also known as flicker noise) refers to a self-similar power spectrum with an exponent close to -1. This definition has been extended to power spectra of the form $E(f) \propto f^{-\alpha}$, with α between 0 and 2. Although this low frequency behavior has been observed in a great variety of systems, no general mechanism has been identified. There exist many theoretical descriptions: existence of a continuous distribution of relaxation times in the system [2,3], fractal Brownian motion [4], intermittent transition to chaos [5] to quote a few.

Exponents between 0 and 2 have been widely observed in spectra of turbulent flows. The standard description of turbulent cascade is that velocity fluctuations have energy between the

✉ F. Pétrélis
petrelis@lps.ens.fr

[1] Laboratoire de Physique Statistique, Ecole Normale Supérieure, CNRS, Université P. et M. Curie, Université Paris Diderot, Paris, France

[2] Helmholtz-Zentrum Dresden-Rossendorf, Bautzner Landstr. 400, 01328 Dresden, Germany

scale of energy injection l_I and the scale of energy dissipation l_d. When Taylor's hypothesis is valid, a power law $f^{-5/3}$ is observed on a frequency range that is limited by τ_I^{-1} and τ_d^{-1}, where τ_I (respectively τ_d) is the turn-over time of eddies of size l_I (resp. l_d). This power law is related to eddies associated to the $k^{-5/3}$ Kolmogorov spectrum that sweep the measurement point [6]. In the case of wall turbulence, a $1/f$ spectrum has been observed and related to the advection of structures with a $1/k$ spectrum in wavenumber [7]. However, we emphasize that the above spectra are not the ones observed in the low frequency limit. Other power-law behaviors have been reported for frequencies much smaller than the inertial range, i.e. frequencies that are not related to any spatial scale through a Taylor's hypothesis. Such $1/f^\alpha$ fluctuations have been reported for the pressure [8] and the velocity [9] in von Karman swirling flows, for the magnetic field in magnetohydrodynamic turbulence [10–13], for two-dimensional turbulence [14] and also in the solar wind [15]. It has been shown in these studies that $1/f$ noise is related to the slow dynamics of coherent structures that have been widely studied because of their impact on the statistical properties of turbulent velocity field [16]. However, the explicit relation between the low frequency spectrum and the dynamics of coherent structures has been emphasized only recently [14].

A relation between spectra and distributions of bursts has been first discussed by Manneville who studied $1/f$ fluctuations using a mapping which exhibits long laminar phases interrupted by chaotic bursts. He showed that in this deterministic model, $1/f$ noise is related to a self-similar distribution of waiting times between bursts. More precisely, a signal made of bursts with waiting times τ distributed as τ^{-2}, exhibits a f^{-1} spectrum [5]. In a similar approach, Geisel et al. showed that the power spectrum is given by $E(f) \sim f^{-\alpha}$ for a distribution of waiting times given by $P(\tau) \sim \tau^{\alpha-3}$ [17]. Lowen and Teich then extended this result by including the case of random transitions between symmetric states [18].

It is tempting to apply the previous approach to coherent structures coexisting with turbulent fluctuations. This requires to identify transitions between different states. It has been shown that two-dimensional turbulence (respectively von Kármán flows) display transitions between symmetric states [19,20] (respectively between different flow patterns [9]). We show here that the statistical properties of these transitions are responsible for the $1/f$ fluctuations. We consider three different fields: the large scale circulation in two-dimensional turbulence, the magnetic field generated by a von Kármán flow of liquid sodium and pressure fluctuations in a turbulent von Kármán swirling flow. For all these systems, we demonstrate that $1/f$ noise is related to the dynamics of large scale coherent structures that transition between different states. The distribution of the time spent in one of the states follows a power law with an exponent that sets the value of the exponent of the power spectrum.

The organization of the paper is as follows. In Sect. 2 the renewal theory and the prediction of Lowen and Teich [18] are recalled. A qualitative argument is presented to understand the connection between the $1/f$ spectrum and self-similar distribution of waiting times. In Sect. 3, we analyze the data obtained in three experiments in the light of these theoretical predictions.

2 Renewal Process with Heavy-Tailed Distributions of Interevent Durations

2.1 Description

A renewal process is a stochastic process defined by a sequence of N events associated to a series of durations $(\tau_i)_N$, with τ random, positive and independent identically distributed

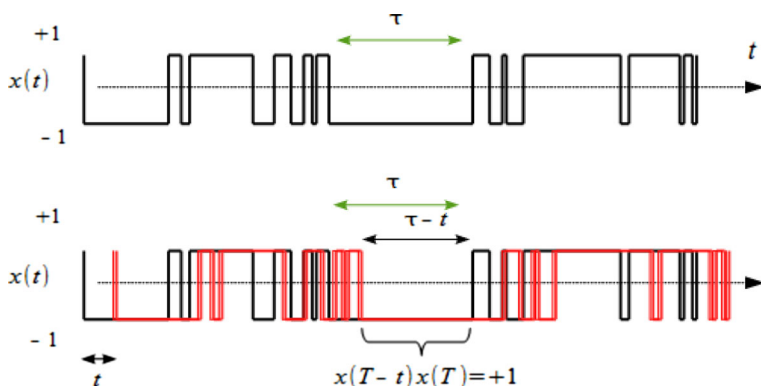**Fig. 1** *Top* renewal process defined by random transitions between two-states, associated to the values $x = \pm 1$. *Bottom* the auto-correlation function $C(t)$ is given by the integration of the product $x(T)x(T - t)$, which is mostly made of long phases of constant polarity and phases of fast oscillations. The former phases contribute to the long-range correlation

variables. In the following, the events correspond to transitions between two states S called A and B and τ_i is the time spent in one state after the $i - 1$ event. We introduce the variable $x(t)$, such that $x(t) = x_A$, when $S = A$ and $x(t) = x_B$, when $S = B$. The distribution of the duration τ is P_A for the state A and P_B for the state B. The process is symmetric when $P_A = P_B$. Figure 1 (top) illustrates a symmetric renewal process with $x_A = 1$ and $x_B = -1$.

The power spectrum of x is defined by

$$E(f) = \frac{1}{T_f} \langle \hat{x}(f) \hat{x}^*(f) \rangle \quad \text{with} \quad \hat{x}(f) = \int_0^{T_f} x(t) e^{i2\pi f t} dt \tag{1}$$

where $\langle \cdot \rangle$ is the average over the realizations and $T_f = \sum_{i=1}^{N} \tau_i$ is the duration of the process, that ultimately tends to infinity. In this study, we are interested in self-similar power spectra with $E(f) \sim f^{-\alpha}$, and $0 < \alpha < 2$.

2.2 Relation Between the Exponents α and β

We start with a qualitative argument to explain how the distribution $P(\tau) \sim \tau^{-\beta}$ controls the value of the exponent α [18]. To wit, we first obtain the auto-correlation $C(t)$ of x and then we calculate the power spectrum of x using the Wiener-Khinchin theorem. The autocorrelation function $C(t)$ is defined by

$$C(t) = \langle x(0)x(t) \rangle \tag{2}$$

The Wiener–Khinchin theorem states that the Fourier transform of $C(t)$ converges to $E(f)$ for $T_f \to \infty$. We consider a symmetric process with $x_A = 1$ and $x_B = -1$ as sketched in Fig. 1. We fix $\beta > 2$ so that $\langle \tau \rangle < \infty$. For an ergodic process and $T_f \gg \langle \tau \rangle$, the auto-correlation $C(t)$ is obtained by

$$C(t) = \frac{1}{T_f} \int_0^{T_f} x(T - t)x(T)dT \tag{3}$$

We observe that the product $x(T)x(T - t)$ is composed of fast oscillations and long periods of constant polarity, due to long phases of duration τ in $x(T)$ (Fig. 1, bottom). We assume that only the phases with $\tau > t$ contribute to the autocorrelation with a contribution $\tau - t$. In other words, the average contributions of short phases with $\tau < t$ vanish. It follows that
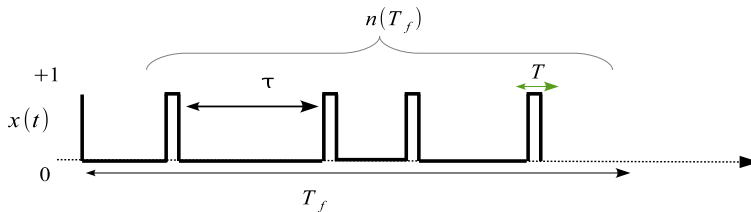
Fig. 2 Time series displaying bursts from $x = 0$ to $x = 1$. The process is asymmetric and the duration of the low amplitude phases is distributed according to a power law, $P \sim \tau^{-\beta}$. In contrast the large amplitude phases have durations that are not distributed following a heavy-tailed distribution

the autocorrelation is approximated by

$$C(t) \simeq \frac{1}{T_f} \int_t^{T_f} (\tau - t) n(\tau) d\tau \quad \text{for} \quad \langle \tau \rangle \ll t \ll T_f \tag{4}$$

with $n(\tau)$ the number of phases of duration τ, which is equal to $P(\tau) T_f / \langle \tau \rangle$, with $T_f / \langle \tau \rangle$ the total number of events. Then, Eq. (4) becomes

$$C(t) \simeq \frac{1}{\langle \tau \rangle} \int_t^{T_f} (\tau - t) P(\tau) d\tau. \tag{5}$$

If $P(\tau)$ is an exponential function, the autocorrelation function is also an exponential function, as expected for a Poisson process. For $P(\tau) \sim \tau^{-\beta}$ and $\beta > 2$, the autocorrelation scales as $C(t) \sim t^{-\beta+2}$. Finally, the power spectrum $E(f)$ is given by the Fourier transform of $C(t)$

$$E(f) \sim f^{\beta-3} \int u^{-\beta+2} e^{-2\pi u i} du \tag{6}$$

with the change of variable $u = ft$ and for $T_f \to \infty$. We thus obtain $\alpha = 3 - \beta$. The result is extended to $1 < \beta < 2$ [18,21] by considering a distribution with $P \sim \tau^{-\beta}$ for $\tau_i \ll \tau \ll \tau_e$, and zero otherwise or exponentially distributed. For a symmetric process ($P_A = P_B$), the power spectrum is then given by

$$E(f) \sim \begin{cases} f^{-(3-\beta)} & \text{for} \quad 1 < \beta < 3 \\ \ln(\tau_i f) & \text{for} \quad \beta = 3 \end{cases} \tag{7}$$

for $\tau_e^{-1} \ll f \ll \tau_i^{-1}$.

Bursting processes can also be considered. The signal $x(t)$ is composed of short intermittent bursts of duration T separated by intervals τ distributed as $P(\tau) \sim \tau^{-\beta}$ (see Fig. 2). The result differs from the symmetric case when $\beta < 2$. Consider a time series for which $x(0) = 1$. Let $n(T_f)$ be the number of bursts within a time interval of length T_f. We estimate

$$I = \int_0^{T_f} x(0) x(t) dt \simeq n(T_f) T \tag{8}$$

The number of bursts is roughly, $n(T_f) = T_f / \langle \tau \rangle_{T_f}$ where $\langle \tau \rangle_{T_f}$ is the average duration of the $x = 0$ phases when we consider a time series of duration T_f. For $\beta < 2$, $\langle \tau \rangle_{T_f}$ does not tend to a constant at large T_f, which obviously results from the divergence of the first moment of the distribution P. Then an estimate of $\langle \tau \rangle_{T_f}$ is given by

$$\langle \tau \rangle_{T_f} = \int_0^{T_f} \tau P(\tau) d\tau \simeq T_f^{2-\beta} \tag{9}$$

We thus have $n(T_f) \simeq T_f^{\beta-1}$. Averaging I over realizations and differentiating with respect to T_f, we obtain the autocorrelation function as $C(t) \propto t^{\beta-2}$. The exponent of the power spectrum then satisfies $\alpha = \beta - 1$.

To sum up, the predictions for the power spectrum of a bursting process are [18,21]

$$E(f) \sim \begin{cases} f^{-(\beta-1)} & \text{for} \quad 1 < \beta < 2 \\ \ln(f\tau_i)^{-2}f^{-1} & \text{for} \quad \beta = 2 \\ f^{-(3-\beta)} & \text{for} \quad 2 < \beta < 3 \\ \ln(\tau_i f) & \text{for} \quad \beta = 3 \end{cases} \tag{10}$$

We note that for symmetric or bursting processes, α is equal to $3 - \beta$ for $\beta > 2$. It implies that the effect of asymmetry in the process is relevant only for distributions with $\beta < 2$.

These results hold for a range of frequencies f corresponding to the inverse range of durations τ over which $P(\tau)$ displays a power law. In particular, if $P(\tau)$ displays a cut-off for time larger than τ_e, $1/f$ noise may be observed down to the low frequency cutoff τ_e^{-1}.

3 Application to Turbulent Time Series

We now illustrate how coherent structures generate a $1/f$ spectrum in three different configurations involving turbulent flows. After shortly describing the experiments, we identify transitions in the time series. We then show that the measured exponents α of the power spectrum and β of the distribution of waiting times follow the theoretical predictions of Sect. 2, which depend on the value of β and on the nature of the process (bursting or symmetric). We recapitulate the results in the following table (Table 1).

3.1 Two-Dimensional Turbulence

We have performed an experiment that consists in driving a flow with an electromagnetic force in an electrically conducting fluid [14]. A thin layer of liquid metal (Galinstan) of thickness $h = 2$ cm, is contained in a square cell of length L = 12 cm. The cell is located inside a coil producing a uniform vertical magnetic field of strength up to $B_0 = 0.98$T. A DC current I (0–200 A) is driven through the bottom of the cell using a periodic array of 8 electrodes with alternate polarities. The current density **j** is radial close to each electrode. The Lorentz force $\mathbf{f}_L = \mathbf{j} \times \mathbf{B}_0$ creates locally a torque. For small injected currents, the laminar flow corresponds to an array of 8 counter-rotating vortices shown in Fig. 3 (center, top). The flow remains mostly two-dimensional, due to Ohmic dissipation of the perturbations with velocity dependence along the direction of the magnetic field.

Table 1 Summary of the experimental results

System	Variable	Process	α	β	Relation
Two-dimensional turbulence	Velocity	Symmetric	0.7	2.25	$\alpha = 3 - \beta$
Von Kármán sodium dynamo	Magnetic field	Bursting	0.5	2.5	$\alpha = 3 - \beta$
Von Kármán flow	Pressure	Bursting	0.6	1.58	$\alpha = \beta - 1$

We recall the experimental configuration (first column), the measured variable (second column), the nature of the process (third column), the measured exponents α and β and the expected relation between them, depending on the value of β and on the nature of the process
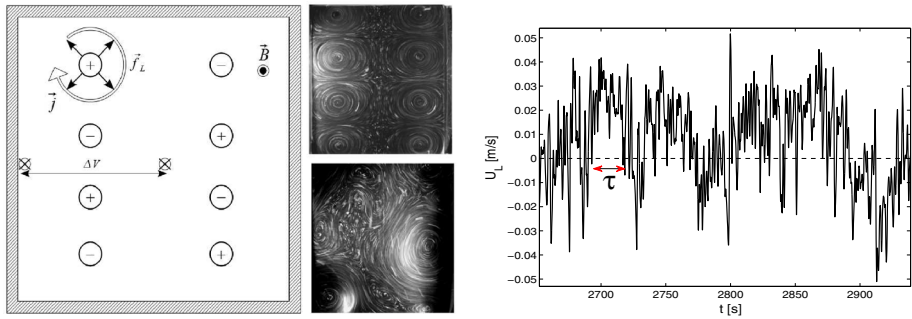
Fig. 3 *Left* Schematics of the experimental set-up. The Lorentz force close to the electrodes generates an array of height counter-rotating vortices in the laminar regime (*center top picture*). The turbulent flow (*center bottom picture*) is characterized by coherent vortices forcing a large scale circulation. The flow rate is measured between the center and the wall, using the induced voltage ΔV. *Right* time series $U_L(t)$ of the flow rate divided by the distance $L/2$ for $Rh = 15$
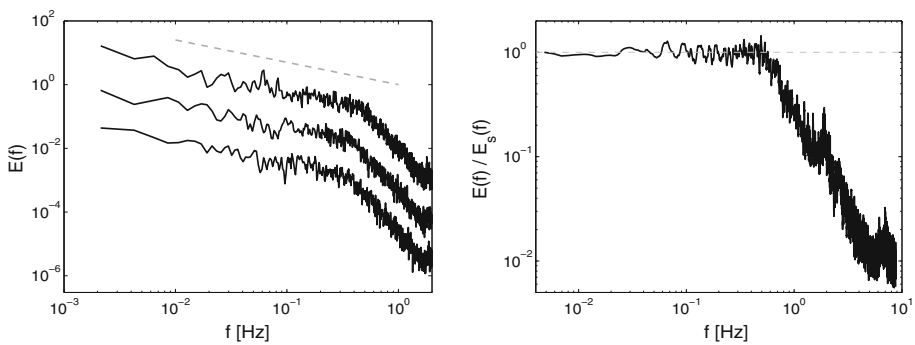

Fig. 4 *Left* frequency power spectra $E(f)$ of $U_L(t)$ for $Rh = 16, 19, 24$ (from *bottom* to *top*). For clarity, the spectra have been multiplied by 1, 10 and 100. The $f^{-0.7}$ law is displayed as a *dashed line*. *Right* ratio of the power spectrum of $s(t)$, the sign of $U_L(t)$ and $U_L(t)$, rescaled such that it tends to 1 for $f \to 0$

When the forcing is strong enough, the flow becomes turbulent (Fig. 3, center bottom). Two-dimensional turbulence is characterized by an inverse cascade of energy [19]. The energy is transferred to large scales and a circulation at the scale of the box displays lifetimes larger than its turn-over time. The dissipation is mostly provided by the friction of the bulk flow with the bottom boundary layer for very large Reynolds number Re. The ratio of the forcing to the large scale dissipation that results from bottom friction is given by the dimensionless number Rh. Typically, the flow becomes turbulent for $Rh \simeq 5$.

The velocity measurements are performed with a pair of electric potential probes (Fig. 3): one is located in the middle of the cell and the other one close to the lateral wall. The probes measure a potential difference ΔV, due to the integral contribution of the local electromotive force $E = -\mathbf{u} \times \mathbf{B}_0$. Thus, $\Delta V = \phi_L B_0$, with ϕ_L the flow rate between the center and the wall of the cell. We use the velocity amplitude U_L, defined by $U_L = \phi_L/(L/2)$. The voltage is sampled at a frequency rate $f_r = 10Hz$. A typical time series of U_L is shown in Fig. 3 (right) for $Rh = 15$.

For $15 \leq Rh \leq 28$, these time series exhibit a clear $1/f^{\alpha}$ power spectrum over nearly two decades for $f < 3.10^{-1}Hz$ (Fig. 4, left). This frequency range is smaller than the inverse of the large eddy turnover time $\tau_L = L/\sigma_U$, with σ_U the standard deviation of U_L. It is
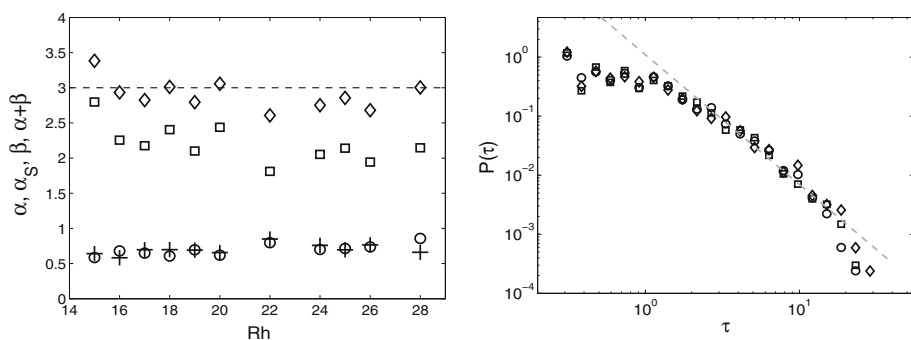
Fig. 5 *Left* Exponents α (*circle*) and β (*square*) for times series with different *Rh*. The exponent of the spectrum of $s(t)$ (*plus*) and the sum $\alpha + \beta$ (*diamond*) are also displayed. *Right* distribution $P(\tau)$ of the waiting time τ between sign changes for $Rh = 16, 19, 24$. The *dashed line* indicates $\tau^{-2.25}$

also smaller than the damping rate τ_D^{-1} due to large scale friction which is the most efficient dissipation mechanism at large scale. For the range of *Rh* studied here, these two time scales are comparable, i.e. $\tau_L \simeq \tau_D$, with typical values between 1 and 6 seconds. Thus the observed $1/f$ spectrum is not directly related to the energy cascade, but to the coherent dynamics of the large scale circulation. A systematic study of the exponents α, defined by $E(f) \sim f^{-\alpha}$, shows that their value is almost constant and equal to 0.7 for $Rh \in [15, 28]$ (black circles, Fig. 5, left).

A closer inspection shows that the time series U_L is composed of long phases of constant polarity of duration τ superimposed with random fluctuations. In Fig. 3, we highlight a phase of constant polarity with duration τ of 20 s (see the event indicated by a double-arrow). The inverse of this time τ^{-1} belongs to the frequency range of the $1/f$ spectrum. Due to the symmetry of the forcing, U_L displays random transitions between both polarities. In order to show that these transitions generate the $1/f$ noise, we transform the signal U_L into a two-state signal $s(t)$, which is defined by the sign of U_L, i.e. $s \equiv \text{sign}(U_L)$. A typical time series is composed of one thousand transitions from one direction of rotation to the other. The ratio of the power spectrum of U_L to the one of s is reported in Fig. 4 (right) and is almost constant over the frequency range corresponding to the $1/f$ spectrum. Thus both power spectra have the same behaviour at low frequency. A systematic study of the exponent α_s of the power spectrum of $s(t)$ (black cross in Fig. 5) shows that its value is very close to the exponent α (black circles). This implies that the slow dynamics of U_L, which is responsible for the $1/f$ noise, is mostly contained in $s(t)$.

We calculate the probability density function of the duration between sign changes of s and report it in Fig. 5 (right). The distributions exhibit a power-law behavior for durations $\tau \in [2, 20]s$ corresponding to frequencies $f \in [5.10^{-2}, 5.10^{-1}]$ Hz included in the range over which $1/f$ noise is observed. We recover the association of a self-similar distribution of interevent durations with a self-similar spectrum of the time series. A systematic measurement of the exponent β (black square, Fig. 5, left), defined by $P(\tau) \sim \tau^{-\beta}$, shows that $\beta \simeq 2.25$.

The sum $\alpha + \beta$ (diamonds in Fig. 5, left) remains close to 3, as predicted by equation (7) for a symmetric renewal process. All the previous results confirm that the random changes of the sign of U_L with waiting time distributed as $P \sim \tau^{-2.25}$, is at the origin of the observed $1/f$ noise.
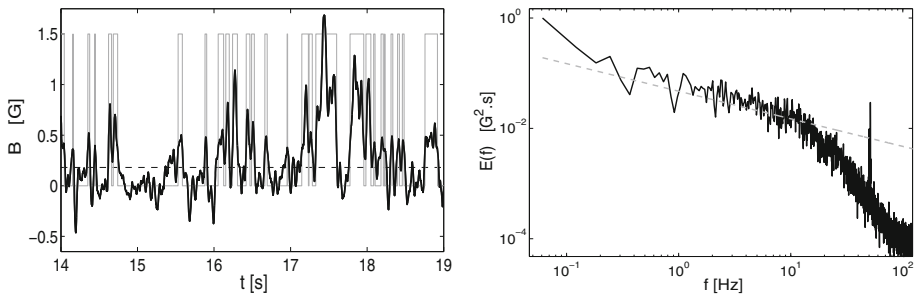
Fig. 6 *Left* time series $B(t)$ of the azimuthal magnetic field, fluctuating around its mean value (*dashed line*). The *grey line* corresponds to the bursting process $s(t)$ extracted from $B(t)$. *Right* power spectrum of $B(t)$ displaying a $f^{-0.5}$ behavior at low frequency (*dashed line*)

3.2 Dynamics of the Magnetic Field Generated by a von Kármán Flow of Liquid Sodium

The generation of magnetic field by a turbulent flow of liquid sodium has been widely studied in the VKS experiment, described in detail in Ref. [12]. The flow is driven by two counter-rotating coaxial impellers in a cylindrical vessel (see Fig. 8, left). When the rotation rate of the impellers is larger than a critical frequency F_c, a magnetic field is generated by a self-sustained induction process, called the dynamo effect. The large scale magnetic field is mostly a stationary axial dipole with superimposed magnetic fluctuations due to the strong turbulence of the flow. $1/f$ noise in the power spectrum of the magnetic field has been reported in dynamo regimes [12] and also below the dynamo threshold when an external magnetic field is imposed to the turbulent flow of liquid sodium [10]. We consider below the dynamo case but the same analysis hold for both.

We have performed measurements of the azimuthal magnetic field $B(t)$ inside the vessel in the mid-plane between the impellers for $F = 20$ Hz (just above the dynamo threshold). The measurements of the other components of magnetic field show similar results. A time series of $B(t)$ is displayed in Fig. 6 together with its power spectrum which exhibits a $f^{-\alpha}$ spectrum with $\alpha \simeq 0.5$ for $f \in [1, 15]$ Hz, i. e. below the inertial frequency range. For $f > 20$ Hz, the power spectrum scales as $f^{-11/3}$, due to the passive stretching of the magnetic field by the small-scale turbulent fluctuations.

As observed in Fig. 6, the magnetic field $B(t)$ displays bursts with amplitudes up to eight times the average value. We first low-pass filter the times series of $B(t)$ below 200 Hz. We then define a two-states signal $s(t)$ by phases of weak and large amplitudes. Among the possible criteria to define a burst, we consider a threshold equal to twice the average value of B, such that above (resp. below) it, the system is in the high (resp. low) amplitude state. The resulting two-states signal $s(t)$ is displayed in Fig 6 (left) in grey. The power spectrum of $s(t)$ (in grey) is compared to the one of B (in black) in Fig. 7 (left). At low frequency, both power spectra follow the same power law. The distribution $P(\tau)$ of waiting times τ between bursts is displayed in Fig. 7 (right). For the range of duration $\tau \in [5.10^{-2}, 25.10^{-2}]s$, $P(\tau)$ follows a power law $\tau^{-\beta}$ with $\beta \simeq 2.5$.

We know from equation (10) holding for burst processes, that α should be equal to $3 - \beta$. The bursting process observed in the VKS experiment for the dynamo case follows this relation with $\alpha = 0.5$ and $\beta = 2.5$.
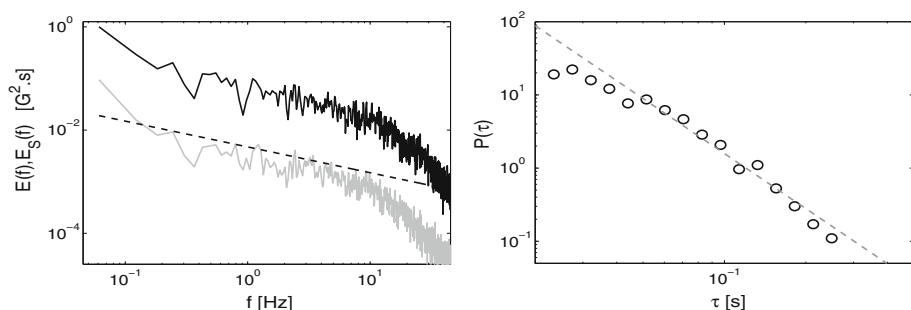
Fig. 7 *Left* power spectrum of $B(t)$ (*black line*) and $s(t)$ (*grey line*) compared to the law $f^{-0.5}$ (*dashed line*). *Right* distribution of the waiting time τ between bursts, with the law $\tau^{-2.5}$ (*dashed line*)
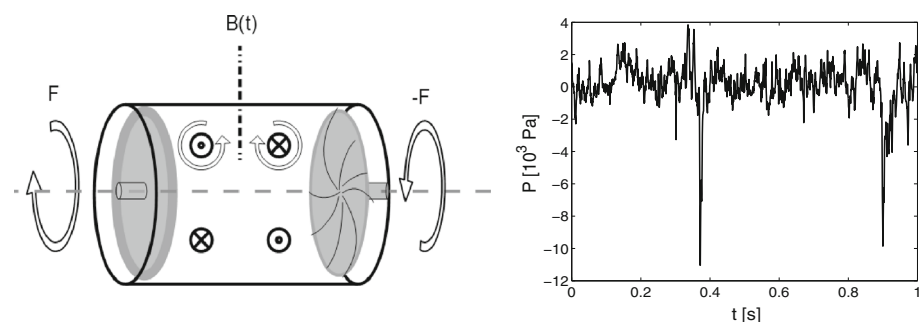

Fig. 8 *Left* Sketch of the VKS and von Kármán experiments: two impellers counter-rotate at frequency F. The *vertical thick line* indicates the location of the magnetic probes in the VKS experiment. *Right* time series $p(t)$ of the wall pressure from Abry et al. [8]

3.3 Pressure Fluctuations in von Kármán Swirling Flows

$1/f$ noise has also been reported for the pressure signal in von Kármán swirling turbulent flows in water [8]. The results presented below are extracted from this reference where a detailed description of the experiment can be found. The pressure $p(t)$ is measured on the lateral boundary of the cylinder. Pressure drops are due to vorticity concentrations passing close to the pressure probe.

The time series of $p(t)$ displaying large pressure drops is shown in Fig. 8 (right). The related power spectrum is shown in Fig. 9 (left, black circles) and exhibits $1/f$ noise at low frequency with an exponent $\alpha = 0.6$. It has been shown in Ref. [8] that removing the pressure drops from the signal using a wavelet technique, almost suppresses the $1/f$ noise from the power spectrum of the filtered signal $\tilde{p}$ (Fig. 8, left, black diamonds). We observe again in this example that the $1/f$ noise results from the bursts. Thus, we define a two-state signal that consists of the long phases of weak amplitude between successive bursts and the short phases of large amplitude pressure drops (the bursts). The distribution of waiting times between successive bursts is displayed in Fig. 9 (right) and exhibits a power law in the range $\log(\tau) \in [-1.7, -0.5]$ (*i.e.* $\tau \in [0.02, 0.3]$ s) roughly corresponding to the frequency range $\log(f) \in [0.6, 1.8]$ (*i.e.* $f \in [4, 60]$ Hz) of the $1/f$ noise. In this range, the fitted exponent is $\beta = 1.58$. We also remark that the distribution has an exponential tail, but only for durations larger than the inverse of the minimum frequency over which $1/f$ noise is observed.
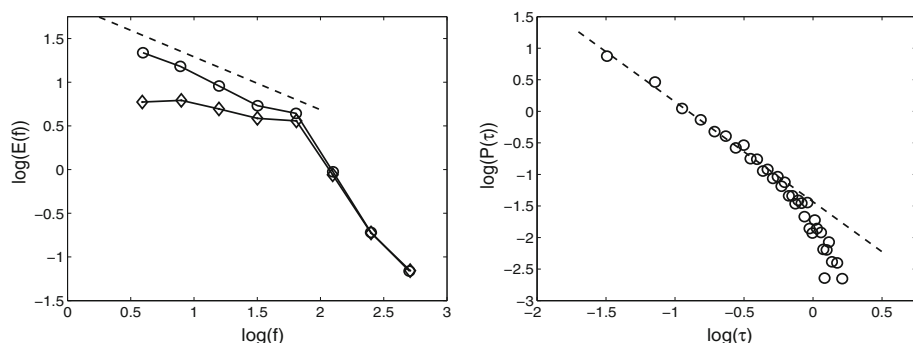
Fig. 9 *Left* power spectra of $p(t)$ (*circle*) and $\tilde{p}$ (*diamonds*), the filtered pressure without bursts. The *dashed line* indicates the law $f^{-0.6}$. *Right* distribution of the waiting time between pressure drops. The law $\tau^{-1.58}$ is displayed with a *dashed line*

In contrast to the previous case, the exponent β is smaller than 2 and the theoretical prediction is then $\alpha = \beta - 1$. Once again, the agreement between the prediction and the fitted exponents is very good with $\beta - 1 = 0.58$ and $\alpha = 0.6$.

4 Conclusion

We have shown that the $1/f$ fluctuations observed experimentally in three different turbulent flows are related to the coherent dynamics of large scale structures, which randomly transition between different states. The dynamics are characterized by the nature of the process (asymmetric bursts or symmetric transitions), and by the power-law distribution of the interevent durations. These two properties fully determine the exponent of the power spectrum.

References

1. Bell, D.A.: A survey of $1/f$ noise in electrical conductors. J. Phys. C **13**, 4425–4437 (1980)
2. Bernamont, J.: Fluctuations in the resistance of thin films. Proc. Phys. Soc. **49**, 138–139 (1937)
3. Van Der Ziel, A.: On the noise spectra of semi-conductor noise and of flicker effect. Physica **16**, 359–372 (1950)
4. Mandelbrot, B.B., van Ness, I.W.: Fractional Brownian motions, fractional noises and applications. SIAM Rev. **10**, 422–437 (1968)
5. Manneville, P.: Intermittency, self-similarity and $1/f$ spectrum in dissipative dynamical systems. J. Phys. **41**, 1235–1243 (1980)
6. Frisch, U.: Turbulence: The Legacy of AN Kolmogorov. Cambridge university press, Cambridge (1995)
7. Perry, A.E., Henbest, S., Chong, M.S.: A theoretical and experimental study of wall turbulence. J. Fluid Mech. **165**, 163–199 (1986)
8. Abry, P., et al.: Analysis of pressure fluctuations in swirling turbulent flows. J. Phys. II **4**, 725–733 (1994)
9. Ravelet, F., Chiffaudel, A., Daviaud, A.: Supercritical transition to turbulence in an inertially driven von Kármán closed flow. J. Fluid Mech. **601**, 339–364 (2008)
10. Bourgoin, M., et al.: Magnetohydrodynamics measurements in the von Kármán sodium experiment. Phys. Fluids **14**, 3046 (2002)

11. Ponty, Y., Politano, H., Pinton, J.F.: Simulation of induction at low magnetic Prandtl number. Phys. Rev. Lett. **92**, 144503 (2004)
12. Monchaux, R., et al.: The von Kármán sodium experiment: turbulent dynamical dynamos. Phys. Fluids **21**, 035108 (2009)
13. Dmitruk, P., et al.: Emergence of very long time fluctuations and $1/f$ noise in ideal flows. Phys. Rev. E **83**, 066318 (2011)
14. Herault, J. : PhD Thesis, *Dynamique des structures coherentes en turbulence magnetohydrodynamique*, Paris 7, (2013). https://tel.archives-ouvertes.fr/tel-00990150/document
15. Matthaeus, W.H., Goldstein, M.L.: Low-frequency $1/f$ noise in the interplanetary magnetic field. Phys. Rev. Lett. **57**, 495 (1986)
16. Hussain, A.K.M.: Coherent structures and turbulence. J. Fluid Mech. **173**, 303–356 (1986)
17. Geisel, T., Zacherl, A., Radons, G.: Generic $1/f$ noise in chaotic Hamiltonian dynamics. Phys. Rev. Lett. **59**, 2503 (1987)
18. Lowen, S.B., Teich, M.C.: Fractal renewal processes generate $1/f$ noise. Phys. Rev. E **47**, 992 (1993)
19. Sommeria, J.: Experimental study of the two-dimensional inverse energy cascade in a square box. J. Fluid Mech. **170**, 139–168 (1986)
20. Gallet, B., et al.: Exact two-dimensionalization of low-magnetic-Reynolds-number flows subject to a strong magnetic field. Geophys. Astrophys. Fluid Dyn. **106**, 468–492 (2012)
21. Niemann, M., Kantz, H., Barkai, E.: Fluctuations of $1/f$ noise and the low-frequency cutoff paradox. Phys. Rev. Lett. **110**, 140603 (2013)